COMPARISON OF GERMANIUM BIPOLAR JUNCTION TRANSISTOR MODELS FOR REAL-TIME CIRCUIT SIMULATION

Ben Holmes

Sonic Arts Research Centre,
School of Electronics, Electrical Engineering
and Computer Science
Belfast, U.K
bholmes02@qub.ac.uk

Martin Holters

Department for Signal Processing and
Communications,
Helmut Schmidt University
Hamburg, Germany
martin.holters@hsu-hh.de

Maarten van Walstijn

Sonic Arts Research Centre,
School of Electronics, Electrical Engineering
and Computer Science
Belfast, U.K
m.vanwalstijn@qub.ac.uk

ABSTRACT

The Ebers-Moll model has been widely used to represent Bipolar Junction Transistors (BJTs) in Virtual Analogue (VA) circuits. An investigation into the validity of this model is presented in which the Ebers-Moll model is compared to BJT models of higher complexity, introducing the Gummel-Poon model to the VA field. A comparison is performed using two complementary approaches: on fit to measurements taken directly from BJTs, and on application to physical circuit models. Targeted parameter extraction strategies are proposed for each model. There are two case studies, both famous vintage guitar effects featuring germanium BJTs. Results demonstrate the effects of incorporating additional complexity into the component model, weighing the trade-off between differences in the output and computational cost.

1. INTRODUCTION

Recent developments in processing power have allowed for real-time simulation of many audio circuits at a physical level, prompting the search for component models that achieve the highest accuracy whilst maintaining real-time compatibility. In the field of VA modelling, circuits featuring BJTs have been modelled successfully with a variety of different component models. Simplified models of the BJT are useful in applications featuring many BJTs. A notable case is exemplified in the modelling of the Moog Ladder filter in which current gain is presumed infinite, reducing a stage of two BJTs to one nonlinear equation [1]. In circuits featuring fewer BJTs, the large-signal Ebers-Moll model has been used [2]. This component model has been used in circuit models of complete guitar pedals, including wah-wah [3] and phaser effects [4].

Despite having been replaced by their silicon counterpart in most areas of electronics, vintage germanium BJTs (GBJTs) have remained consistently popular in guitar pedals, particularly fuzz effects. In previous work, two circuits featuring GBJTs have been studied: the Fuzz-Face [5] and Rangemaster [6] guitar pedals, both using the Ebers-Moll BJT model. However, each differs in how the parameters are derived: the Fuzz Face using parameters extracted from a datasheet, and the Rangemaster using parameters extracted through an optimisation procedure based on input/output data. Comparisons between the output of the circuits and the models demonstrate a good fit in certain regions of operation, though there are errors present in both models which remain unattributed. The component with the most complex behaviour in each circuit is the BJT which suggests it as a likely source of error.

A step further in complexity from the Ebers-Moll model is a possible solution to this issue. Significant improvements have been published, including: the Gummel-Poon model [7], the VBIC

model [8], and the MEXTRAM model [9]. These models have not yet featured in the field of VA, leaving the question of what difference they may make.

The aim of this paper is to provide an analysis of GBJTs within audio circuits for the purpose of VA modelling. This analysis consists of two primary sections: firstly the characterisation of models based on measurements, followed by the analysis of each model within the context of an audio circuit model. The analysed models include the Ebers-Moll model and models similar to Gummel-Poon, considering both additional DC and AC effects. Procedures for DC parameter extraction from measurements are discussed for all models. We revisit the case studies already presented: the Dallas Rangemaster Treble Booster and the Dallas Arbiter Fuzz-Face. In order to focus the analysis firmly on the differences between the BJT models, comparisons are made only between circuit models, as any separate circuit measurement would be subject to a range of further system variances and errors.

The rest of the paper is structured as follows: Section 2 describes the compared BJT models, Section 3 discusses extraction procedures for the DC parameters, Section 4 covers the case studies, the methodology, and results of the BJT model comparison, and Section 5 concludes with suggestions for modellers working on circuits featuring GBJTs.

2. BJT MODELS

This section describes the BJT models used in the analysis. Both GBJTs that are studied are PNP, which is reflected in the description of the models. The difference with an NPN model is only in notation, not behaviour.

In this work we define the term 'external' to refer to behaviour modelled by additional components i.e. resistors and capacitors. 'Internal' will refer to the remaining terms, modelled as voltage controlled current sources. This is illustrated by the differences between Figure 1 (a) and (b), in which the BJT in (b) is modelled by (a). External components values are modelled as being independent of the BJT bias point i.e. constant. Combination of the internal and external components will result in three models: the Ebers-Moll model, a DC Gummel-Poon model, and an AC Gummel-Poon (including capacitances).

Table 1 provides a reference for the name of each parameter in each model. The effect of changes in each parameter value will be discussed through the explanation of the extraction procedure in Section 3. Only necessary discussion is included about each BJT model; for a more comprehensive description see e.g. [10].
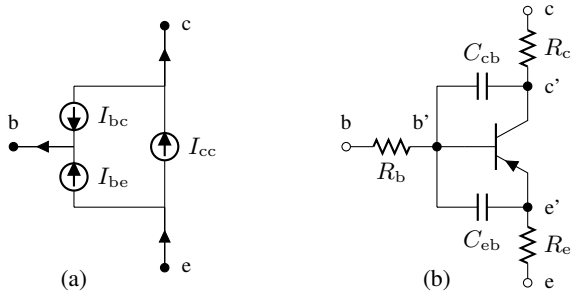
Figure 1: (a) *Internal model schematic representation.* (b) *Complete model using additional components.*

2.1. Ebers-Moll

The Ebers-Moll model can be understood as modelling the two *pn* junctions of the BJT as back to back diodes with coupling between junctions. This can be expressed as

$$I_f = I_s \left(e^{\frac{V_{eb}}{N_f V_t}} - 1\right), \quad I_r = I_s \left(e^{\frac{V_{cb}}{N_r V_t}} - 1\right) \quad (1)$$

$$I_{cc} = I_f - I_r, \quad I_{be} = \frac{1}{\beta_f} I_f, \quad I_{bc} = \frac{1}{\beta_r} I_r \quad (2)$$

$$I_c = I_{cc} - I_{bc}, \quad I_b = I_{be} + I_{bc} \quad (3)$$

where I_c and I_b are the currents through the collector and base, and V_{eb} and V_{cb} are the voltages across the emitter- and collector-base junctions. It is important to note that the remaining voltages and currents can be found by Kirchoff's circuit laws, i.e. $V_{ec} = V_{eb} - V_{cb}$ and $I_e = I_c + I_b$.

Intermediate terms are used in the description of the model to facilitate its extension and describe its behaviour in important regions of operation. I_f and I_r are forward and reverse currents which can be considered independent when the controlling voltage of the other current is zero. The terms I_{cc}, I_{be} and I_{bc} directly describe the schematic representation of the model, illustrated in Figure 1(a) as three current sources. Upon extension to the internal Gummel-Poon this representation remains the same, only requiring modification of the functions each current source represents.

2.2. Internal Gummel-Poon

To form the internal Gummel-Poon model several effects are added which change the behaviour in both low and high current regions, and also in response to changes in V_{ec}. Terms defined in (1) hold for the extended model whereas the intermediate current terms in (2) are replaced. The internal Gummel-Poon is then expressed as [11]

$$I_{be} = \frac{1}{\beta_f} I_f + I_{se}(e^{\frac{V_{eb}}{N_e V_t}} - 1) \quad (4)$$

$$I_{bc} = \frac{1}{\beta_r} I_r + I_{sc}(e^{\frac{V_{cb}}{N_c V_t}} - 1) \quad (5)$$

$$I_{cc} = \frac{2}{q_1(1 + \sqrt{1 + 4q_2})}(I_f - I_r) \quad (6)$$

where

$$q_1 = \frac{1}{1 - \frac{V_{eb}}{V_{ar}} - \frac{V_{cb}}{V_{af}}}, \quad q_2 = \frac{I_f}{I_{kf}} + \frac{I_r}{I_{kr}}. \quad (7)$$

The new terms in I_{be} and I_{bc} improve the modelling of the low current behaviour often referred to as leakage. A dependence of

I_c on V_{ec} is introduced through q_1 where two parameters control an increase to I_c relative to the positive and negative values of V_{ec} (consider the junction voltage that is dominant in each case). Finally, a current gain roll-off is introduced to the model through the inclusion of q_2 which reduces I_c at high voltage values.

To reduce the internal Gummel-Poon to the Ebers-Moll model, parameters must be set to specific values: $I_{se} = I_{sc} = 0$ and $V_{af} = V_{ar} = I_{kf} = I_{kr} = \infty$.

2.3. External components

Five additional components are included in this work: a resistance at each terminal and a capacitance between both the base-emitter junction and the base-collector junction. Figure 1(b) illustrates the inclusion of these components to the internal BJT model.

More comprehensive models include two capacitances between each junction [10], both dependent upon the voltage across the junction; however, these are non-trivial to model using most VA techniques. Because of this, and also to reduce the difficulty in the measurement procedure, constant capacitance values were extracted from the datasheets of each GBJT.

3. PARAMETER EXTRACTION

DC parameter values for each model were extracted from measurements of GBJTs. The extraction strategy consists of a direct extraction followed by several targeted optimisations. This strategy is based on existing work [12, 13], but both of these tools are implemented in commercial systems which were unavailable. Therefore a straightforward approach was developed to operate on minimal measurements, with dedicated extraction procedures for the Ebers-Moll and Gummel-Poon models.

3.1. Measurement Strategy

Three sets of measurements were performed on each BJT: forward and reverse Gummel plots, which exposes the BJT behaviour in forward and reverse bias conditions, and the common-emitter output characteristic. Each measurement is designed to enable direct extraction of certain parameters by exposing specific behaviour. The circuits required for each measurement are illustrated in Figure 2. Table 2 contains the sourced currents and voltages for each measurement.

The common-emitter output characteristic is measured by specifying a base current, sweeping V_{ec}, and measuring I_c. This is repeated for different values of I_b providing several snapshots of the relationship between V_{ec}, I_b and I_c.

The forward Gummel plot fixes V_{ec} at a positive bias while V_{eb} is swept over a range and both I_c and I_b are measured. This is similar for the reverse Gummel plot, where V_{ec} is biased negatively, V_{cb} is swept, and I_e and I_b are measured. The applied methodology is described in [12], where V_{ec} is biased between 2 V and half of the maximum voltage supplied in the common-emitter output characteristic. This creates a direct relationship between the common-emitter characteristic at that value of V_{ec} and the Gummel plots, such that the voltages and currents should all be equal. This approach therefore biases the BJT in the active regions which provides confidence that the model will fit all measurements.

A Keithley 2602B Source Measure Unit was used to perform the measurements, enabling simultaneous measurement and sourcing of current and voltage. However, it should be noted that the Gummel plots can be measured using only voltages by placing a

Table 1: *List of all parameters and extracted values from both the OC44 and AC128; constraints used in the intermediate optimisation stages; initial values used for parameters that were not found through direct extraction.*

Parameter		Extracted Values				Optim. Constraints		Init. Values
		OC44		AC128		Lower Lim.	Upper Lim.	
		E.M.	G.P.	E.M.	G.P.			
I_s	Saturation current	2.029 µA	1.423 µA	23.75 µA	20.66 µA	-	-	-
β_f	Forward current gain	108.1	307.0	44.90	229.6	50	250	-
β_r	Reverse current gain	8.602	20.27	4.568	14.66	3	20	-
N_f	Forward ideality factor	1.062	1.022	1.168	1.133	-	-	-
N_r	Reverse ideality factor	1.105	1.025	1.171	1.140	-	-	-
(V_t)	Thermal voltage	25.5 mV	25.5 mV	25.5 mV	25.5 mV	-	-	-
V_{af}	Forward Early voltage	-	8.167 V	-	19.68 V	-	-	-
V_{ar}	Reverse Early voltage	-	14.84 V	-	88.28 V	-	-	-
I_{kf}	Forward knee current (gain roll-off)	-	43.82 mA	-	463.0 mA	10 µA	500 mA	-
I_{kr}	Reverse knee current (gain roll-off)	-	611.7 mA	-	241.5 mA	10 µA	500 mA	-
I_{se}	BE junction leakage current	-	30.54 nA	-	2.190 µA	0.1 fA	1 mA	$I_s/2$
I_{sc}	BC junction leakage current	-	213.5 nA	-	7.546 µA	0.1 fA	1 mA	$I_s/2$
N_e	BE junction leakage emission coefficient	-	1.316	-	1.796	0.5	4	2.3
N_c	BC junction leakage emission coefficient	-	1.258	-	1.364	0.5	4	2.4
R_b	Base resistance	-	32.83 Ω	-	1.885 Ω	1 Ω	250 Ω	25 Ω
R_e	Emitter resistance	-	968.7 mΩ	-	306.4 mΩ	0.1 nΩ	2 Ω	10 mΩ
R_c	Collector resistance	-	989.9 µΩ	-	1.727 µΩ	-	-	10 mΩ
C_{eb}	Emitter-base capacitance	-	410 pF	-	-	-	-	-
C_{cb}	Collector-base capacitance	-	10 pF	-	100 pF	-	-	-

Table 2: *Ranges of the inputs to each measurement circuit. Specific values of I_b are provided on each measurement plot.*

Meaurement	Input	OC44	AC128
Forward	V_{eb}	0 - 0.7 V	0 - 0.8 V
Gummel	V_{ec}	2 V	2 V
Reverse	V_{cb}	0 - 0.8 V	0 - 0.8 V
Gummel	V_{ec}	–2 V	–2 V
Common	I_b	3 - 50 µA	26 - 1000 µA
Emitter	V_{ec}	–5 - 5 V	–5 - 5 V

shunt resistor over which to measure the voltage drop. This is important as it reduces the equipment required for measurements, and as will be shown provides enough information to characterise the Ebers-Moll model.

3.2. Direct Extraction

Direct extraction of parameters is used to provide initial estimates upon which optimisation can then be performed. Estimates can be made using simplifications as the optimisation performs the majority of the extraction. However, it is essential to start the optimisation process in a position within the parameter space close to the optimum to avoid local minima which may halt the optimisation without providing the best model fit.

3.2.1. Ebers-Moll parameters

The Ebers-Moll parameters are extracted from the measured Gummel plots. Figure 3 illustrates the effects of the forward parameters and the saturation current I_s. This behaviour is equivalent in the reverse plot with the reverse parameters meaning that both regions can be described by analysing only one, in this work the forward region. To simplify the extraction procedure, the opposite current term, in this case, I_r is neglected, which is only valid if $V_{cb} = 0$. As the measurement strategy actually enforces $V_{cb} < 0$ there will

be an error introduced into the direct extraction, but the error is small, typically $I_r \leq I_s$. Further, this error is removed during the optimisation stages where there is no model simplification.

The thermal voltage V_t can be found directly through measuring the temperature of the room in which the measurement is taken. This relies on the assumption that the measurements are taken in such a way that avoids the BJT being heated by the current passing through it, and that the BJT is allowed to settle at room temperature prior to measurement. Using the temperature in kelvin T_K, $V_t = T_K \frac{k}{q}$ where k is Boltzmann's constant and q is the charge on an electron.

Following this, the ideality factor N_f can be found through finding the gradient of the log of I_c. While the model shown in Figure 3 is ideal, in measurements of BJTs the gradient of I_c will not be constant so it is important to find a suitable point at which to perform the extraction. One suitable method is to find the first minimum of the absolute value of the second derivative of I_c. Neglecting constant terms from I_f in (1) allows the formation of the expression

$$\frac{d\log(I_c)}{dV_{eb}} = \frac{1}{N_f V_t}. \tag{8}$$

Rearranging this equation provides a value for N_f. A value for I_s can then be found at the same value of V_{eb}, by solving the simplified expression of I_c for I_s, i.e.

$$I_c = I_s \exp\left(\frac{V_{eb}}{N_f V_t}\right), \quad I_s = \exp\left(\log(I_c) - \frac{V_{eb}}{N_f V_t}\right). \tag{9}$$

Examining this equation for when $V_{eb} = 0$ it is clear that I_s is the *y*-intercept of the Gummel-plot, as illustrated in Figure 3.

The extraction of β_f relies on the relationship between I_c and I_b, which from (1-3) can be expressed as $I_c = \beta_f I_b$. This relationship is illustrated in Figure 4. As V_{eb} approaches zero, I_b decreases such that β_f increases very rapidly. This does not provide practical values of β_f so values of β_f beneath the first turning point with respect to V_{eb} can be excluded. The maximum of the β_f is then used as the directly extracted parameter value.
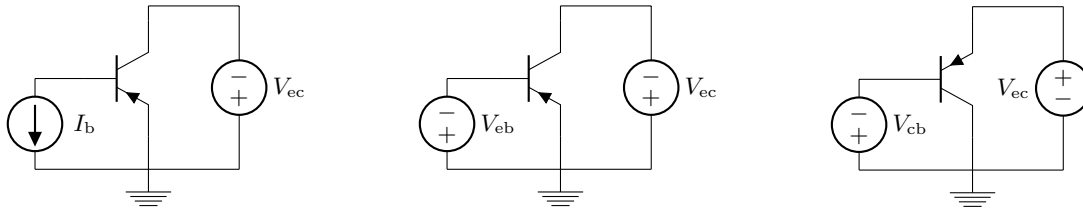
Figure 2: *Measurement circuits for parameter extraction. Common-Emitter (left), Forward Gummel (middle), Reverse Gummel (right).*
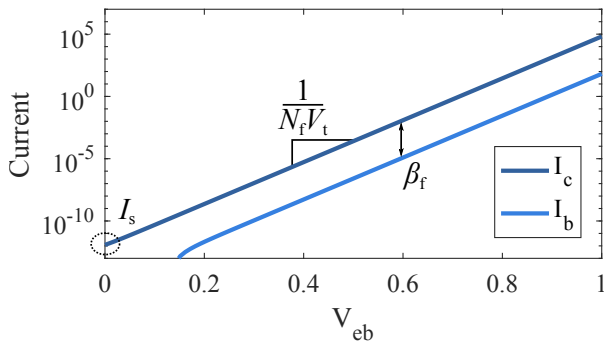

Figure 3: *Example forward Gummel plot of the Ebers-Moll model illustrating the effects of the forward parameters N_f, β_f and also I_s. Currents I_c and I_b are plotted logarithmically in the current range against linear V_{eb}.*
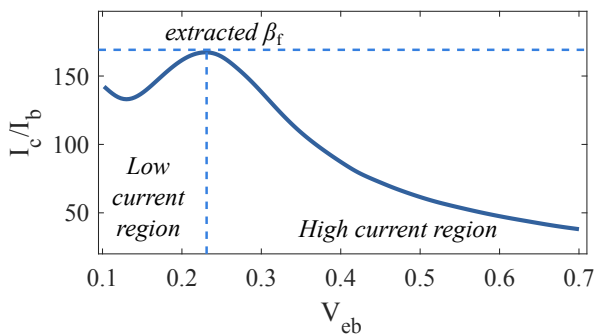

Figure 4: *Example plot showing the relationship between I_c/I_b and V_{eb}. A nominal value of β_f is extracted from the maximum value, shown by the dashed line. High and low current effects cause reduction of β_f.*

3.2.2. Gummel-Poon parameters

Values for I_{kf} and I_{kr} can be extracted from the current gain plots, the forward of which is illustrated in Figure 4. The extracted values for I_{kf} and I_{kr} are given by the value of I_c and I_e at which the current gain falls to half of its maximum value (respectively). If necessary the curve can be extrapolated to find a value.

It was not found necessary to implement a direct extraction technique for each parameter as initial values could be found through manually tuning the leakage parameters and terminal resistances. Due to the similarity of the GBJTs being modelled, several parameters could be initialised at the same value for each GBJT and provide a good starting point for the optimisation stage of the extraction. The values for each parameter initialised using this method are shown in Table 1.

3.3. Optimisation Stages

After completing the direct extraction, each model's fit to measurements was optimised. Each optimisation was performed on a specific input range, selected to emphasise the relevant behaviour for each set of parameters being optimised. The ranges used can be found in Table 3. Different strategies were required for characterising the Ebers-Moll model and DC Gummel-Poon.

Two optimisation algorithms were used from MATLAB's optimisation toolbox, `fminsearch` which uses the Nelder-Mead simplex method [14], and `fmincon`, which uses the interior-point method [15]. The Nelder-Mead simplex method is useful in this scenario due to it's ability to handle discontinuous surfaces. This enabled the use of objective functions that would return an infinite value if the parameters supplied were negative, preventing non-physical parameter sets. Experimentally it was found that this combination provided better convergence properties than using the interior-point method with a similar boundary. However, the interior-point method was useful in scenarios in which more complex boundaries were required to ensure the parameters retrieved would be a suitable starting point for the next simulation. The final stage of characterising each model was performed with the Nelder-Mead simplex method.

The same objective function was used for each optimisation with the only change being the data compared. The objective value is normalised with respect to both the number of data points and the values of the data points. An example of this can be expressed by

$$R(\theta, y) = \frac{1}{N} \sum_{n=1}^{N} \left(\frac{y[n] - \hat{y}(\theta)[n]}{y[n]} \right)^2 \qquad (10)$$

where R is the objective value, y is the measured data, $\hat{y}(\theta)$ is the modelled data for a given parameter set θ, and N is the number of data points.

3.3.1. Ebers-Moll

Following the direct extraction, one optimisation stage was used in the extraction of the Ebers-Moll parameters. This was performed on the Gummel plots, using a low voltage range (see Table 3) to match the first 'ideal' region in which the gradient of the collector current is constant.

3.3.2. Gummel-Poon

The optimisation procedure for the DC Gummel-Poon model is illustrated in Figure 5. After the direct extraction stage, three stages of optimisations are used. The intermediate optimisation stages use constraints implemented using the interior-point method. Constraints for the intermediate optimisations can be seen in Table 1.

The first optimisation stage works on the current gain of the BJTs, given by e.g. I_c/I_b for the forward case. This significantly
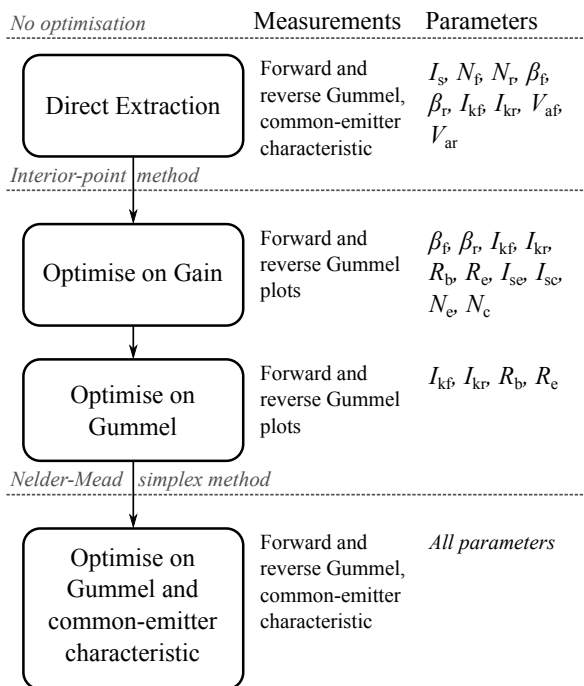
Figure 5: *Optimisation strategy used to extract the parameters of the Gummel-Poon model. The arrow indicates the flow of stages of extraction. The resultant parameters of each stage are passed on to the next.*

reduces the effects of I_s, V_{af}, V_{ar}, R_c, N_f, N_r, reducing the parameter set and thus the number of dimensions in the optimisation. A second stage was used to further tune a subset of these parameters to the Gummel plots. Finally, all parameters were optimised against all of the data sets. A weighting was applied to the objective function in the final optimisation, making the objective value of the common-emitter characteristic $10\times$ higher than that of the Gummel plots.

3.4. Results

Multiple GBJTs were used in the comparison: 4 AC128 and 3 OC44 BJTs. Figures 6 and 7 show the results of the best fit of the DC Gummel-Poon to the measurements as determined by the objective function of the final optimisation. As these models had the best fit to the data, they were used in the comparison in the case studies. See Table 1 for the parameters of each model.

Thermal effects were noticed in the measurements despite considerations to reduce the effects. Post processing was used to reduce the observable effect of these; however there remains a possibility that some thermal error remains in the measurements which would affect the extracted parameters.

In the high-current region of the Gummel-plots the model deviates from the measurements. During the measurement stage, a current limit was enforced to prevent damage to components or the measurement system, set slightly above the maximum current specified by the GBJT datasheets. This limited the amount of high-current data that could be gathered. Further, the common-emitter plots were taken at low currents to ensure they were close to that of the 'ideal' region of operation, which reduces the amount of data about the high-current region. If the measurements were to

Table 3: *Voltage ranges upon which each optimisation for both models were performed. Gummel plots were used in both the penultimate and ultimate stages for the Gummel-Poon model, and are labelled 1 and 2 to differentiate.*

Model	Measurement	Input	Lower limit	Upper limit
Ebers-Moll	Gummel plots	V_{eb}, V_{cb}	10 mV	200 mV
Gummel-Poon	Current gain	V_{eb}, V_{cb}	110 mV	700 mV
	Gummel plots 1	V_{eb}, V_{cb}	100 mV	700 mV
	Gummel plots 2	V_{eb}, V_{cb}	50 mV	600 mV
	Common-emitter	V_{ec}	−5 V	5 V

be repeated it might be sensible to increase the base currents in the common-emitter characteristic, and consider increasing the current limit.

4. CASE STUDIES

The schematics of the Dallas Rangemaster and Dallas Arbiter Fuzz-Face can be found in Figures 8 and 9 respectively. These case studies were selected because each biases the BJT in different regions, exhibiting different behaviour. Three tests were performed on each case study: informal listening tests, waveform comparisons, and a comparison of the computational requirements. Each circuit was modelled using the Nodal DK-method (for reference see e.g. [3]) although it should be noted that the use of a different simulation technique would yield similar results for both audio and waveform comparisons. Computation time would however require evaluation for different simulation techniques. For each test all potentiometers of both case studies were set to maximum. Other potentiometer settings were tested but are omitted as they illustrate no substantial difference from those presented.

4.1. Informal listening tests

Several guitar signals were processed by both case studies at $8\times$ oversampling as a means of comparing each model. Listeners agreed that differences could be heard between each model, with the Ebers-Moll model having the most high frequency content due to distortion and the AC Gummel-Poon having the least. Audio examples can be found on the first author's website[1].

4.2. Waveform comparison

An objective comparison of each BJT model is achieved here using time-domain waveforms. Sinusoids at different frequencies and amplitudes were processed by both case studies and each model. To remove transient behaviour from the results, the final period of each of these signals are shown in Figure 10 and 11. Plots at 1200 Hz show the largest difference for the AC effects, illustrating the low-pass type behaviour of the capacitances. Differences due to the increased DC complexity are most prominent at lower amplitudes.
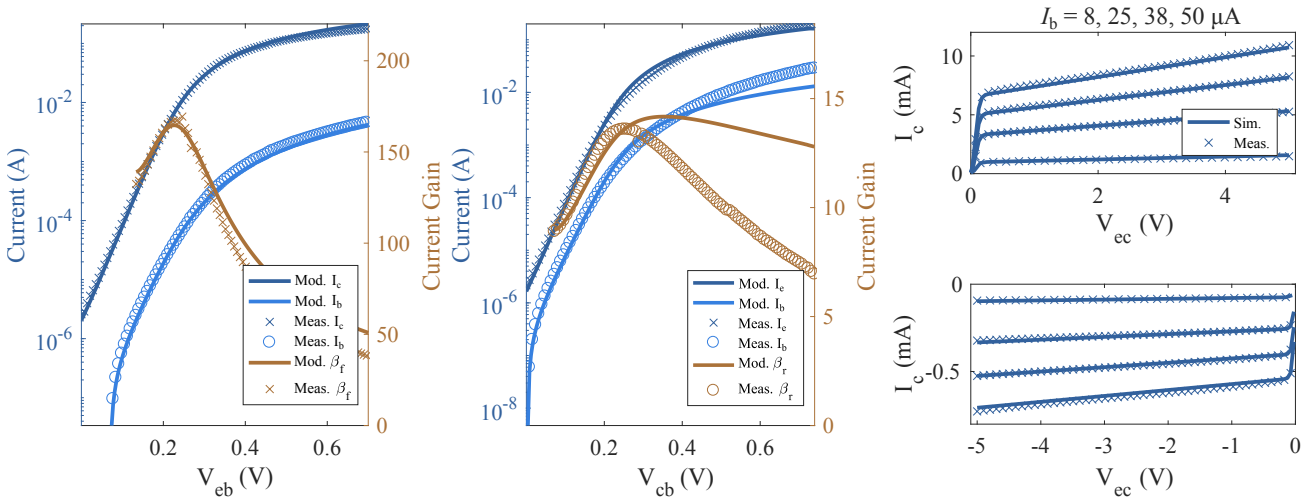
---

[1] http://bholmesqub.github.io/DAFx17/

Figure 6: *Forward and reverse Gummel plots and the common-emitter characteristic of the OC44 BJT.*

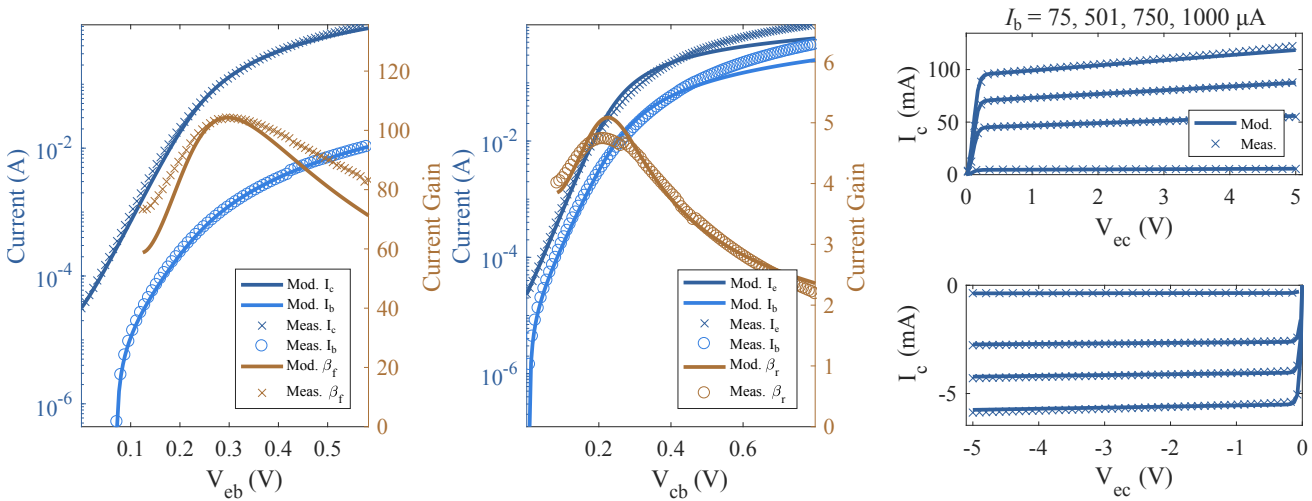Figure 7: *Forward and reverse Gummel plots and the common-emitter characteristic of the AC128 BJT.*
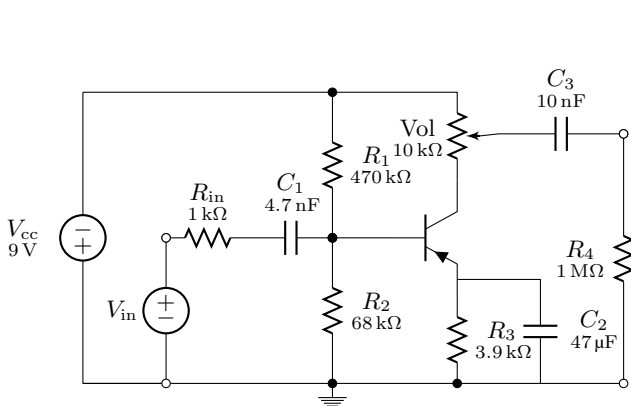

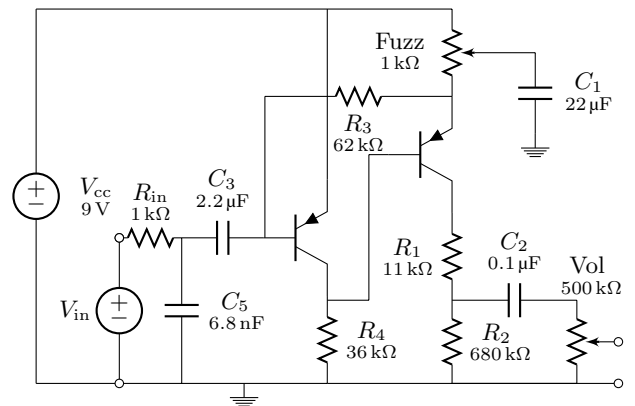Figure 8: *Schematic of the Rangemaster circuit.*

Figure 9: *Schematic of the Fuzz Face circuit.*

Table 4: *Simulation time required to process one second of signal, average iterations per sample, and sub-iterations per sample of circuit models processing a guitar chord using different BJT models. The Rangemaster was tested over a peak voltage range of $0.1 - 2\,\mathrm{V}$, the Fuzz-Face over a range of $10 - 100\,\mathrm{mV}$.*

Model	Rangemaster		Fuzz-Face	
	Sim. time/s (ms)	Mean Iter./Sub-iter.	Sim. time/s (ms)	Mean Iter./Sub-iter.
DC E.M.	95.9	3.53/0.20	341.6	3.62/0.04
AC E.M.	75.8	3.52/0.13	376.5	3.60/0.01
DC G.P.	371.8	3.47/0.07	819.1	3.04/0.03
AC G.P.	357.0	3.45/0.05	769.9	2.99/0.01

4.3. Computational efficiency

To understand the cost of increasing the complexity of the BJT model, computational requirements of each model were compared. The nonlinear equation of the circuit models was solved using damped Newton's method as described in [16], which uses an inner iterative loop to aid in convergence. This provides three metrics: time needed for one second of simulation, average iterations, and average sub-iterations.

A fourth model was included for this test: the Ebers-Moll model with C_{eb} and C_{cb} (AC Ebers-Moll) to provide an improved assessment of the cost of the capacitances. A guitar signal was processed by both case studies and each BJT model, with the peak amplitude of the signal set to 20 different levels. Computation time was then measured by MATLAB's `tic`/`toc` stopwatch functions. The results are shown in Table 4. It is clear from the results that increasing the DC complexity causes a significant increase in computation time, whereas including additional capacitances carries little cost. As iterations and sub-iterations decrease with increasing model complexity the increase in computation must be due to the increased complexity of evaluating the model equations. Decrease in computation cost when including the capacitances can be attributed to the reduction in high frequencies reducing the stress placed on the iterative solver, outweighing the increase in the complexity from including additional components.

5. CONCLUSION

A comparison of BJT models has been presented with a focus on GBJTs. Each model was characterised by extracting parameters from measured data using a multi-step optimisation strategy. The resultant models were compared through the use of two case study circuits covering both moderately and highly distorted circuit outputs. The circuit models were compared using three metrics: audible and waveform differences, and computational efficiency.

Results show that increase in model complexity does make a change to the behaviour of GBJTs in audio circuit models. This work has primarily focused on improving DC characterisation; however, the results show that AC effects are at least equally important. The improved DC characterisation has a significant increase in computational cost whereas the cost of the AC effects are minimal. These results indicate that any first extension to the Ebers-Moll model should be AC effects, and further extensions should then concern DC effects.

The core motivating factor for implementing and characteris-

ing more sophisticated BJT models was to reduce the error present in VA circuits featuring GBJTs. A fitting next step is to now use these models in conjunction with the design of models based on specific circuits. An implementation of the Gummel-Poon model has been included in ACME.jl[2] emulation tool for modellers interested in further investigation.

6. REFERENCES

[1] A. Huovilainen, "Non-linear digital implementation of the Moog ladder filter," in *Proc. of the International Conference on Digital Audio Effects (DAFx-04)*, Naples, Italy, 2004, pp. 61–64.

[2] J. J. Ebers and J. L. Moll, "Large-signal behavior of junction transistors," *Proceedings of the IRE*, vol. 42, no. 12, pp. 1761–1772, 1954.

[3] M. Holters and U. Zölzer, "Physical Modelling of a Wah-Wah Pedal as a Case Study for Application of the Nodal DK Method to Circuits with Variable Parts," in *Proc. of the 14th Internation Conference on Digital Audio Effects*, Paris, France, Sept. 2011, pp. 31–35.

[4] F. Eichas, M. Fink, M. Holters, and U. Zölzer, "Physical Modeling of the MXR Phase 90 Guitar Effect Pedal," in *Proc. of the 17 th Int. Conference on Digital Audio Effects*, Erlangen, Germany, Sept. 2014, pp. 153–156.

[5] K. Dempwolf and U. Zölzer, "Discrete State-Space Model of the Fuzz-Face," in *Proceedings of Forum Acusticum*, Aalborg, Denmark, June 2011, European Acoustics Association.

[6] B. Holmes and M. van Walstijn, "Physical model parameter optimisation for calibrated emulation of the Dallas Rangemaster Treble Booster guitar pedal," in *Proc. of the 19th Internation Conference on Digital Audio Effects*, Brno, Czech Republic, Sept. 2016, pp. 47–54.

[7] H. K. Gummel and H. C. Poon, "An integral charge control model of bipolar transistors," *Bell System Technical Journal*, vol. 49, no. 5, pp. 827–852, 1970.

[8] C. C. McAndrew, J. A. Seitchik, D. F. Bowers, M. Dunn, M. Foisy, I. Getreu, M. McSwain, S. Moinian, J. Parker, D. J. Roulston, and others, "VBIC95, the vertical bipolar inter-company model," *IEEE Journal of Solid-State Circuits*, vol. 31, no. 10, pp. 1476–1483, 1996.

[9] R. Van der Toorn, J. C. J. Paasschens, and W. J. Kloosterman, "The Mextram bipolar transistor model," *Delft University of Technology, Technical report*, 2008.

[10] I. Getreu, *Modeling the Bipolar Transistor*, Tektronix, 1976.

[11] A. Vladimirescu, *The SPICE book*, J. Wiley, New York, 1994.

[12] F. Sischka, "Gummel-Poon Bipolar Model: Model description, parameter extraction.," *Agilent Technologies*, 2001.

[13] J. A. Seitchik, C. F. Machala, and P. Yang, "The determination of SPICE Gummel-Poon parameters by a merged optimization-extraction technique," in *Proc. of the 1989 Bipolar Circuits and Technology Meeting*. 1989, pp. 275–278, IEEE.

[14] J. C. Lagarias, J. A. Reeds, M. H. Wright, and P. E. Wright, "Convergence properties of the Nelder–Mead simplex method in low dimensions," *SIAM Journal on optimization*, vol. 9, no. 1, pp. 112–147, 1998.

[15] R. H. Byrd, J. C. Gilbert, and J. Nocedal, "A Trust Region Method Based on Interior Point Techniques for Nonlinear Programming," *Mathematical Programming*, vol. 89, no. 1, pp. 149–185, 2000.

[16] B. Holmes and M. van Walstijn, "Improving the robustness of the iterative solver in state-space modelling of guitar distortion circuitry," in *Proc. of the 18th International Conference on Digital Audio Effects*, Trondheim, Norway, Dec. 2015, pp. 49–56.
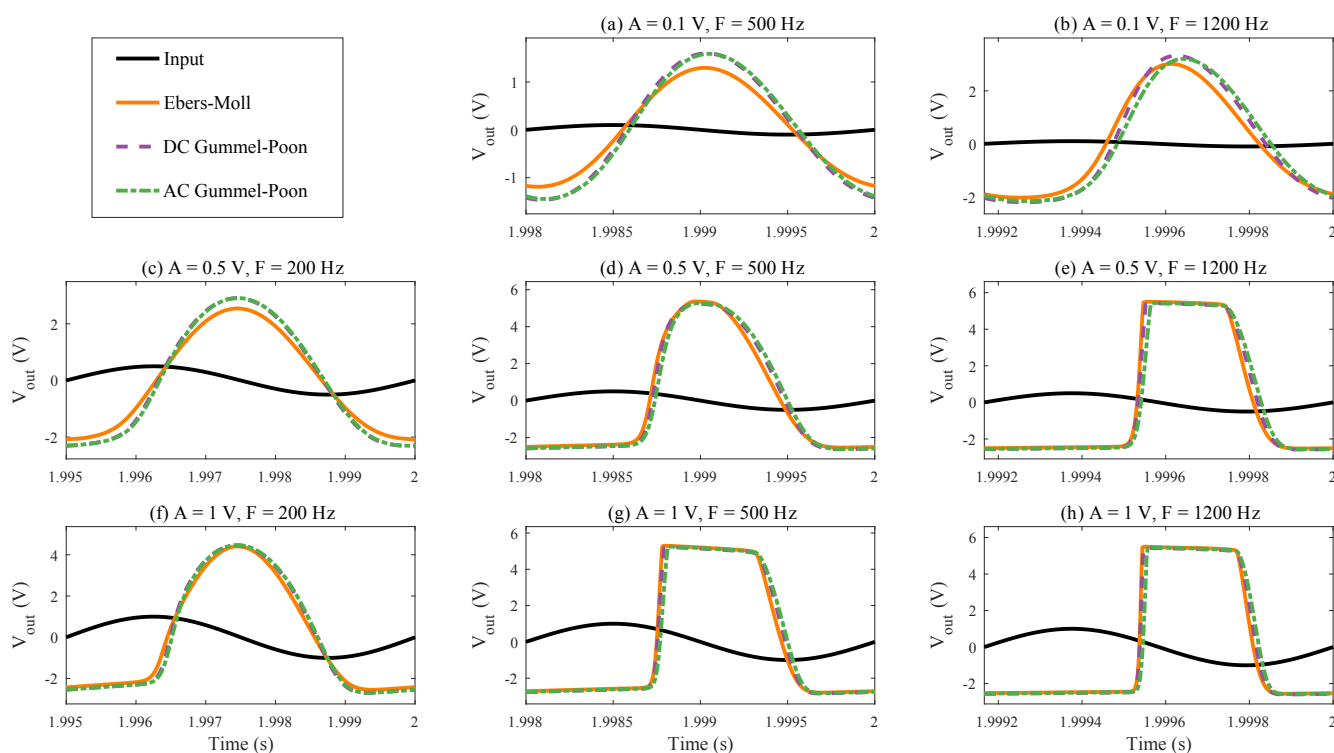
---

[2]https://github.com/HSU-ANT/ACME.jl

Figure 10: *Single cycles of the Rangemaster output's response to a sinusoidal input signal.*
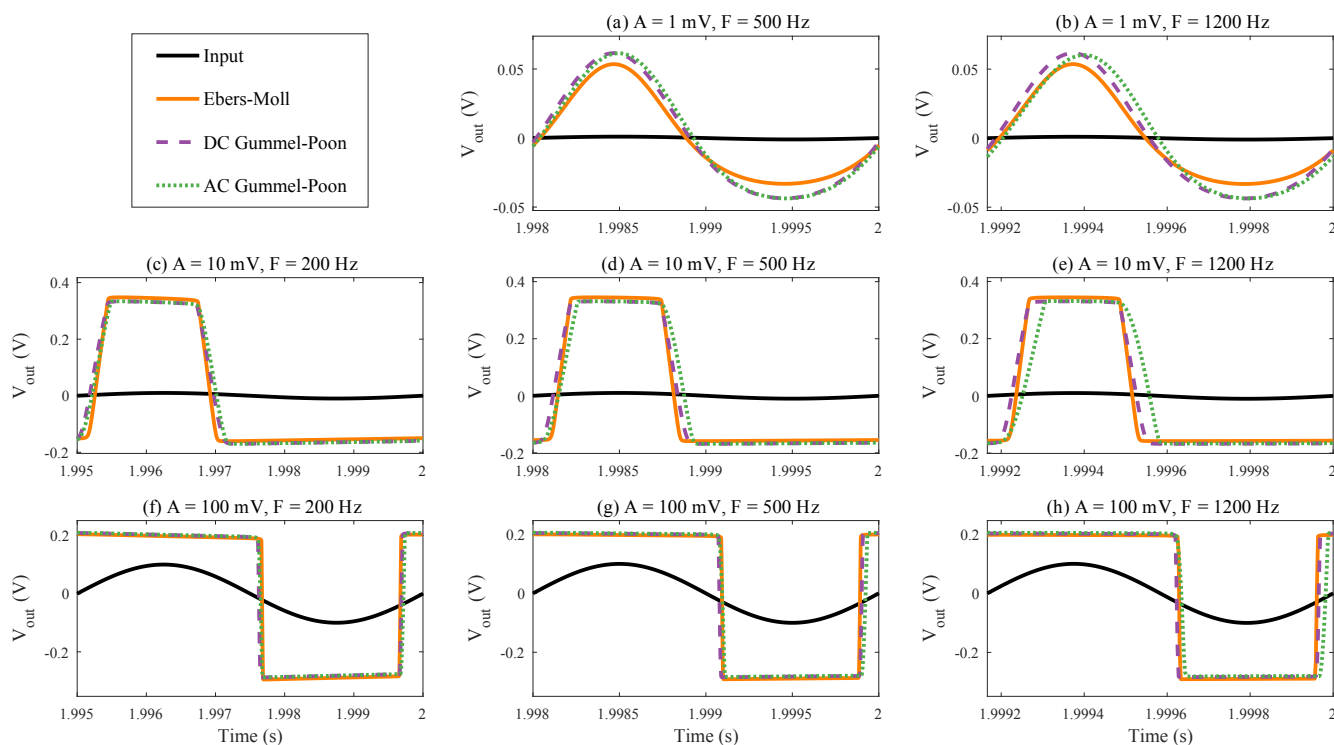
Figure 11: *Single cycles of the Fuzz Face output's response to a sinusoidal input signal. The fuzz control of the circuit was set to maximum.*